BIOCHEMISTRY
including biophysical chemistry & molecular biology

Article

pubs.acs.org/biochemistry

The Second Ca^{2+}-Binding Domain of NCX1 Binds Mg^{2+} with High Affinity

Vincent Breukels,[†] Albert Konijnenberg,[†] Sanne M. Nabuurs,[†] Wouter G. Touw,[†] and Geerten W. Vuister*[,‡]

[†]Protein Biophysics, Institute for Molecules and Materials, Radboud University Nijmegen, 6525 GA Nijmegen, The Netherlands
[‡]Department of Biochemistry, University of Leicester, Henry Wellcome Building, Lancaster Road, Leicester LE1 9HN, U.K.

Supporting Information

ABSTRACT: We report the effects of binding of Mg^{2+} to the second Ca^{2+}-binding domain (CBD2) of the sodium−calcium exchanger. CBD2 is known to bind two Ca^{2+} ions using its Ca^{2+}-binding sites I and II. Here, we show by nuclear magnetic resonance (NMR), circular dichroism, isothermal titration calorimetry, and mutagenesis that CBD2 also binds Mg^{2+} at both sites, but with significantly different affinities. The results from Mg^{2+}−Ca^{2+} competition experiments show that Ca^{2+} can replace Mg^{2+} from site I, but not site II, and that Mg^{2+} binding affects the affinity for Ca^{2+}. Furthermore, thermal unfolding circular dichroism data demonstrate that Mg^{2+} binding stabilizes the domain. NMR chemical shift perturbations and ^{15}N relaxation data reveal that Mg^{2+}-bound CBD2 adopts a state intermediate between the apo and fully Ca^{2+}-loaded forms. Together, the data show that at physiological Mg^{2+} concentrations CBD2 is loaded with Mg^{2+} preferentially at site II, thereby stabilizing and structuring the domain and altering its affinity for Ca^{2+}.

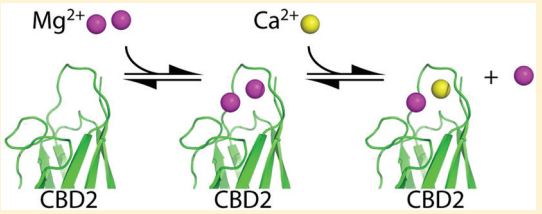

The Na^+−Ca^{2+} exchanger (NCX) is a nearly ubiquitous plasma membrane protein that plays a major role in the extrusion of Ca^{2+}. With three mammalian isoforms and numerous splice variants known, the exchanger is expressed in virtually every tissue.[1,2] To remove Ca^{2+} against the electrochemical gradient, the exchanger utilizes the energy stored in the Na^+ gradient generated by the Na^+/K^+-ATPase.[3] In its dominant mode, NCX exchanges one Ca^{2+} ion for the uptake of three Na^+ ions[4] and the activity is strictly regulated. Only low concentrations above basal levels of the intracellular Ca^{2+} concentration are required for activation, whereas increased intracellular Na^+ concentrations lead to a process called Na^+-dependent inactivation.[5] The allosteric activation by Ca^{2+} is exclusively ascribed to binding of Ca^{2+} ions to two Ca^{2+}-binding domains (subsequently denoted CBD1 and CBD2), whereas the exact site of Na^+ interaction remains to be established. CBD1 and CBD2 reside in the ∼500-amino acid cytosolic loop between transmembrane helices 5 and 6,[6,7] which further contains a third domain tentatively named the α-catenin-like domain (CLD).[8]

The ion affinity of calcium binding proteins must be highly specific for Ca^{2+} as opposed to Mg^{2+}. Cytosolic levels of free Mg^{2+} range from 0.5 to 1.0 mM,[9] whereas cytosolic levels of free Ca^{2+} are around ∼100 nM, which increase up to levels of ∼2 μM near the membrane during processes such as neuronal excitation or muscle contraction.[10] To be functional Ca^{2+} sensors, Ca^{2+}-binding proteins must have an affinity for Ca^{2+} at least 3 orders of magnitude higher than their affinity for Mg^{2+}. Furthermore, Mg^{2+} concentrations are known to fluctuate under pathophysiological conditions and in dialyzed axons,[11] as well as in cardiomyocytes. NCX activity is decreased by high intracellular Mg^{2+} concentrations, possibly by competing with Ca^{2+} at the regulatory sites.[12,13] A more recent in vitro study showed that in both CBD1 and CBD2, Mg^{2+} competes for Ca^{2+},[14] however, with striking differences between the two domains. For CBD1, the apparent affinity for Ca^{2+} decreases at high Mg^{2+} concentrations (5 mM $MgCl_2$), but the number of Ca^{2+} ions bound by CBD1 remains the same. In CBD2, a high Mg^{2+} concentration results in the binding of only one instead of two Ca^{2+} ions, even at an elevated Ca^{2+} concentration, and the apparent affinity for Ca^{2+} at the remaining binding site increases.

To date, detailed atomic structural information about the NCX is limited to CBD1 and CBD2[8,15−19] and the exact mechanism by which they jointly regulate the exchanger in its cellular context remains poorly understood. The NMR and X-ray structures revealed strong structural similarity between CBD1 and CBD2, both consisting of a seven-stranded β-sandwich with the connecting loops forming the Ca^{2+}-binding sites. In NCX1, CBD1 binds four Ca^{2+} ions with high affinity and is considered the primary Ca^{2+} sensor activating the exchanger, whereas CBD2 is capable of binding two Ca^{2+} ions (cf. Figure 1) and deemed responsible for the secondary response.[16]

Recently, we postulated that CBD1 and CBD2 activate the exchanger by acting as an electrostatic switch.[16] In the electrostatic switch mechanism, binding of Ca^{2+} leads to a significantly more positive electrostatic potential of the domain,

Received: July 22, 2011
Revised: September 19, 2011
Published: September 19, 2011

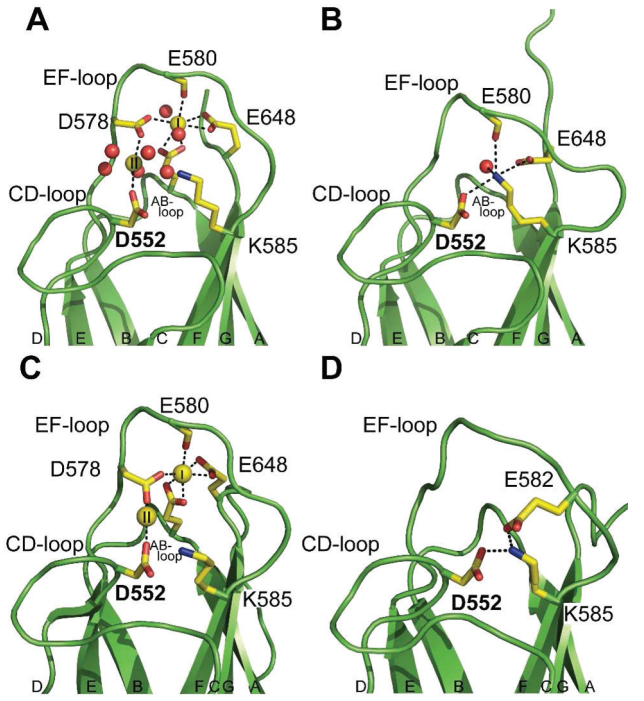

Figure 1. Ribbon diagrams of the X-ray and NMR structures of the apo and Ca^{2+}-bound forms of wild-type CBD2. The main chain is shown as a green ribbon. Red spheres represent water molecules and yellow spheres the primary (I) and secondary (II) Ca^{2+} ions. Strand labels are given at the bottom. (A) Ca^{2+}-bound form X-ray structure (PDB entry 2QVM). The coordination is depicted with dashed lines, and coordinating residues are shown as yellow sticks. (B) Ca^{2+}-free form X-ray structure (PDB entry 2QVK). Lys^{585} points toward the secondary Ca^{2+}-binding site, forming salt bridges with Asp^{552} and Glu^{648} and a hydrogen bond with Glu^{580}, as indicated with dashed lines. (C) Ca^{2+}-bound NMR structure (refined[42] using original restraints of PDB entry 2FWU and Ca^{2+} coordination derived from PDB entry 1QVM). (D) Ca^{2+}-free form NMR structure (PDB entry 2KLS). Lys^{585} forms a salt bridge with Asp^{552} and Glu^{582}, but not with Glu^{648}.

thereby changing the electrostatic interactions with nearby domains. Small angle X-ray scattering data on the NCX showed that the angle between CBD1 and CBD2 changes upon binding of Ca^{2+}, and we proposed that this is due to the altered electrostatic potential of CBD1. By the same mechanism, binding of Ca^{2+} to CBD2 would induce changes to the nearby CLD or membrane part, thereby overcoming the Na^+ inactivation at elevated cytosolic Ca^{2+} levels.[16] Binding of Mg^{2+} to CBD2 would be an additional factor in the electrostatic regulating mechanism, as this also introduces positive charge into CBD2.

We have investigated, using NMR, mutational analysis, circular dichroism (CD), and isothermal titration calorimetry (ITC), the Mg^{2+} binding properties of CBD2. We show that Mg^{2+} preferentially binds to site II of CBD2 and with a much lower affinity to site I. Binding of Mg^{2+} leads to significant structural rearrangements that stabilize the domain. Furthermore, the overall tumbling and backbone dynamics of Mg^{2+}-bound CBD2 determined using ^{15}N relaxation measurements reflect an intermediate bound state of Mg^{2+}-bound CBD2 when compared to its apo and Ca^{2+}-bound forms. Finally, the results show that under physiological conditions, site II of CBD2 is preferentially loaded with one Mg^{2+} ion.

EXPERIMENTAL PROCEDURES

Expression and Purification. NMR, CD, and ITC samples of canine NCX1 CBD2 were made as described previously.[8] In short, all samples were derived from the nucleotide sequences encoding residues 501−657 of canine NCX1 (GenBank entry P23685) that were cloned into a pET23b vector and expressed in *Escherichia coli* BL21(DE3). Cultures were grown at 37 °C until an optical density (OD_{600}) of 0.8−1.0 was reached. Protein expression was then induced for 3 h using 1 mM isopropyl 1-thio-D-galactopyranoside. Purification was facilitated by N-terminal His tags and anion-exchange chromatography (MonoQ, Amersham-Pharmacia). The purity of all samples was >95% as judged by sodium dodecyl sulfate−polyacrylamide gel electrophoresis and ^{15}N HSQC spectra.

ITC. To minimize contaminating divalent cations, all samples were produced in minimal M9 medium with $FeSO_4$ as the only trace element and concentrated in 2.5 mM HEPES (pH 7.0) (Sigma, ultrapure) and 2.5 mM β-mercaptoethanol. The buffers contained <12.5 ppb (~310 nM) contaminating Ca^{2+} as measured by inductively coupled plasma optical emission spectrometry (iCAP 6300, ThermoScientific); 1, 2, or 10 mM $CaCl_2$ and 1 or 10 mM $MgCl_2$ solutions were prepared in a buffer identical to that used for the protein. All ITC measurements were performed at 25 °C using an ITC_{200} (MicroCal) device. In all cases, a 90 μM protein sample was used, as determined using a Nanodrop spectrophotometer ND1000 (Isogen Lifescience). After thermal equilibration, the samples were titrated 38 times with 1 μL injections with a 5 min spacing and at a 500 rpm stirring speed. To correct for background heat, we also titrated divalent cation-containing buffer into buffer. All measurements were performed at least in duplicate to confirm reproducibility.

All data were analyzed using the one-site independent binding model implemented in Origin 7.0 (MicroCal) with the exception of the Ca^{2+} titration to wild-type CBD2 (wt-CBD2) for which a two-site independent model was used.

NMR. All NMR samples were prepared in a manner identical to that used for the ITC samples and concentrated in 20 mM HEPES (pH 7.0) (Sigma, ultrapure), 20 mM β-mercaptoethanol, and 0.03% (w/v) NaN_3 as a preservative to a protein concentration of ~440 μM. All ^{15}N HSQC spectra were recorded on a Bruker Avance III 600 MHz or Varian Inova 800 MHz spectrometer, each equipped with a triple-resonance cryogenic probe. All data were recorded at 33 °C, processed using the NMRPipe program suite,[20] and analyzed using Analysis.[21] Visualization and drawing of molecules were conducted using Pymol.[22]

To assign the ^{15}N HSQC spectra of D552V-CBD2, we conducted the standard triple-resonance experiments [CBCA(CO)NH, HNCACB, HN(CA)HA, and HBHA(CBCACO)NH], which yielded unambiguous resonance identification for 113 of the 157 amides. Significant resonance overlap prohibited complete assignment of D552V-CBD2. A secondary structure prediction was performed using the TALOS+ web server,[23] which shows that the β-sandwich core of D552V-CBD2 is still intact (cf. Figure S5 of the Supporting Information).

To determine the total chemical shift perturbation (CSP), we normalized the ^1H and ^{15}N dimensions according to[24]

$$\Delta\delta_{Tot} = [(W_H\Delta\delta_H)^2 + (W_N\Delta\delta_N)^2]^{1/2} \quad (1)$$

dx.doi.org/10.1021/bi201134u | *Biochemistry* 2011, 50, 8804−8812

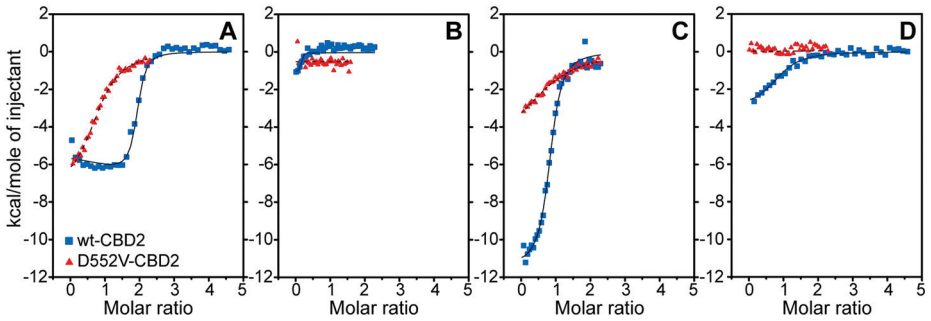

Figure 2. Comparison of the binding thermodynamics of wt-CBD2 (blue squares) and D552V-CBD2 (red triangles), using ITC. (A) Binding isotherms for 2 mM $CaCl_2$ (wild type) or 1 mM $CaCl_2$ (D552V mutant). (B) Binding isotherm of 1 mM $MgCl_2$ with protein. (C) Binding isotherm of 1 mM $CaCl_2$ with protein in the presence of 2 mM $MgCl_2$. (D) Binding isotherm of 1 mM $MgCl_2$ in the presence of 90 μM $CaCl_2$.

Table 1. Thermodynamic Ca^{2+} and Mg^{2+} Binding Parameters for wt-CBD2 and D552V-CBD2 Obtained by Isothermal Titration Calorimetry

sample	ligand	N	K_D (μM)	ΔH (kcal mol^{-1})	ΔS (cal mol^{-1} deg^{-1})
90.0 μM wild type	2 mM $CaCl_2$	1.89 ± 0.05	0.4 ± 1.2[a]	−5.2 ± 3.55[a]	11.7[a]
			1.1 ± 1.4[a]	−7.0 ± 3.57[a]	4.0[a]
90.0 μM wild type with 2 mM $MgCl_2$	1 mM $CaCl_2$	0.85 ± 0.01	3.4 ± 0.4	−11.4 ± 0.2	−13.3
90.0 μM wild type with 90.0 μM $CaCl_2$	1 mM $MgCl_2$	0.89 ± 0.05	14.6 ± 3.4	−3.4 ± 0.2	11.9
90.0 μM D552V	1 mM $CaCl_2$	0.87 ± 0.01	16.1 ± 1.4	−7.4 ± 0.2	−4.7
90.0 μM D552V with 2 mM $MgCl_2$	1 mM $CaCl_2$	0.94 ± 0.07	53.5 ± 9.7	−5.3 ± 0.6	1.8

[a]The two-site binding model gives unreliable results (cf. Results).

where W_H and W_N are weighting factors of 1.00 and 0.154, respectively.

Samples of ~440 μM wt-CBD2 or D552V-CBD2 were titrated with $MgCl_2$ in 10 steps from 0 to 10 mM (Mg^{2+}:protein ratios of 0:1, 0.23:1, 0.47:1, 0.96:1, 1.44:1, 2.05:1, 3.02:1, 4.60:1, 10.4:1, and 26.4:1). Subsequently, the sample was titrated in 10 steps to 10 mM $CaCl_2$ (Ca^{2+}:protein ratios of 0:1, 0.26:1, 0.54:1, 0.96:1, 1.09:1, 1.66:1, 2.25:1, 3.42:1, 5.20:1, 11.7:1, and 29.6:1) while the $MgCl_2$ concentration was kept constant. To obtain per residue K_D values, the CSP data were fitted using a Python routine written in house, assuming simple 1:1 binding as described by André and Linse,[25] using the first nine titration points (see also the Supporting Information).

The ^{15}N-T_1, ^{15}N-$T_{1\rho}$, and {^1H−^{15}N} NOE experiments were conducted at 18.8 T in an interleaved fashion, using a commonly accepted pulse sequence The relaxation delays for the T_1 and $T_{1\rho}$ experiments were 16, 256 384, 512, and 1024 ms and 16, 32, 48, 64, 96, and 128 ms, respectively. The time delay between saturated and unsaturated parts in the {^1H−^{15}N} NOE experiments was set to 13 s. The relaxation data were analyzed as previously described[26] using Tensor2.[27]

Far-UV CD. CD data displayed in panels A and B of Figure 3 were acquired using a Jasco J715 spectropolarimeter. Thermal unfolding of CBD2 was followed at 230 nm. The temperature was increased from 12 or 20 to 95 °C at a rate of 1 °C/min in a 1.5 mL stirred quartz cuvette (path length of 0.4 cm). All CD samples contained 10 μM protein and 1 mM $CaCl_2$, $MgCl_2$, or EDTA in 1 mM HEPES (pH 7.0) and 100 μM β-mercaptoethanol.

To study the ligand concentration dependence of the melting temperature (T_m), we measured the thermal unfolding at 1, 5, 10, 25, 100, 250, 500, and 1000 μM $MgCl_2$ or $CaCl_2$, while adjusting the choline chloride concentration to keep the ionic strength constant. The CD measurements were taken using a Jasco J810 spectropolarimeter, and thermal unfolding was followed at 235 nm. All samples contained 10 μM protein in a 1.5 mL stirred quartz cuvette (path length of 1.0 cm). To reduce the background effects of the buffer, all samples contained 1 mM HEPES (pH 7.0) and 100 μM β-mercaptoethanol. Fitting of the thermal unfolding data assumed a two-state unfolding mechanism (cf. the Supporting Information).

RESULTS

ITC. The AD exon containing the CBD2 splice variant (wt-CBD2) has the ability to bind two Ca^{2+} ions. In the crystal structure of CBD2, Ca^{2+} at site I is coordinated by six carboxylates whereas Ca^{2+} at site II is coordinated by only two [Asp^{552} and Asp^{578} (cf. Figure 1A)]. However, we previously showed that both sites have similar binding affinities, likely as a result of positive cooperativity.[26] To obtain insight into the ion specificity of wt-CBD2, we have measured its binding affinities for both Mg^{2+} and Ca^{2+} using ITC. To differentiate between the two sites, we also investigated a CBD2 mutant in which we mutated Asp^{552} to Val (D552V-CBD2). This mutant lacks a crucial carboxylate coordinating the Ca^{2+} ion in site II. Although mutating an Asp to a Val is not a conserved mutation, this particular D552V mutant has been previously studied via electrophysiology[15] and was shown to constitute a functional exchanger. Figure 2A shows the ITC Ca^{2+} binding curve of wt-CBD2 (blue squares) and D552V-CBD2 (red triangles). The binding curve of wt-CBD2 shows a clear 2:1 binding stoichiometry with binding heats on the order of approximately −6 kcal/mol, as can be judged from the molar ratio at half-maximum and the ΔH at the first injection, respectively. These results are in accordance with the previously measured data.[8] The actual binding stoichiometry (n = 1.89) is slightly lower than the ideal binding stoichiometry (n = 2.0) expected from the crystal structure,[15] and this small deviation might originate from residual Ca^{2+} residing in the sample buffer. As anticipated, the mutant has only one binding site and

dx.doi.org/10.1021/bi201134u | Biochemistry 2011, 50, 8804–8812

displays a slightly increased ΔH of -7.4 ± 0.2 kcal/mol (cf. Table 1), indicating that binding site I in D552V-CBD2 remains intact.

The intracellular free Mg^{2+} concentration in the cell can reach levels up to several millimolar,[9] and we tested Mg^{2+} as a ligand for CBD2. Mg^{2+} appears to bind to wt-CBD2 but not D552V-CBD2 (cf. Figure 2B). Binding of Mg^{2+} to wt-CBD2, however, results in much smaller enthalpic effects compared the effects of Ca^{2+} binding. Furthermore, the Mg^{2+} binding stoichiometry is far below a predicted 1:1 binding ($n = 0.16 \pm 0.04$), and the binding isotherm starts as exothermic and becomes endothermic after the first seven additions. This indicates that at least two processes are involved, and in combination with the small ΔH of the exothermic reaction, this results in the low stoichiometry and a poor fit to the model used. We hypothesize that the endothermic reaction is a low-affinity, nonspecific Mg^{2+} binding process. Moreover, measurements performed at a 10-fold increased ion concentration show that for both Ca^{2+} and Mg^{2+} the endothermic reaction occurs, in the wild type as well as in the D552V mutant (cf. Figure S1 of the Supporting Information).

Under physiological conditions, Ca^{2+} binding occurs in competition with excess Mg^{2+}. Therefore, we measured Ca^{2+} binding in the presence of 2 mM $MgCl_2$ (cf. Figure 2C). Remarkably, at this high Mg^{2+} concentration, we observe a Ca^{2+} binding stoichiometry of 0.85 ± 0.01. Interestingly, the enthalpy of this single binding event ($\Delta H = -11.4 \pm 0.2$ kcal/mol) is much higher when compared to that of Ca^{2+} binding in the absence of $MgCl_2$. In contrast to that of the wild type, the Ca^{2+} binding stoichiometry for the mutant remains 1:1. We observe, however, a loss of binding heat, ΔH decreasing from -7.4 ± 0.2 kcal/mol without Mg^{2+} to -5.3 ± 0.6 kcal/mol in the presence of 2 mM $MgCl_2$. To test if the altered Ca^{2+} binding at 2 mM $MgCl_2$ is a result of the increased ionic strength, we have also measured Ca^{2+} binding for both molecules in the presence of 2 mM choline chloride. We observed that choline chloride does not alter the binding thermodynamics of Ca^{2+} in either of the two molecules (cf. Figure S2 of the Supporting Information) and therefore exclude the effects of ionic strength as the cause of the observed differences.

In an effort to determine the relative binding affinity of Mg^{2+}, we also performed the reverse competition experiment, titrating Mg^{2+} to a partially Ca^{2+}-loaded protein (cf. Figure 2D). At a Ca^{2+}:protein ratio of 1:1, both binding sites are expected to be approximately half-filled.[26] Under this condition, we observe Mg^{2+} binding to wt-CBD2 with a binding stoichiometry of 1:1. Compared to that in the noncompetitive Mg^{2+} binding experiment, the binding heat (ΔH) is increased to -3.4 ± 0.2 kcal/mol. For D552V-CBD2, no binding is observed in the reverse competition experiment. Taken together, the ITC data show that Mg^{2+} cannot displace Ca^{2+} from site I and can bind only at site II.

To compare the results in a more quantitative way, we also fitted all data using MicroCal Origin (cf. Experimental Procedures). Affinities, binding enthalpies, and binding entropies are summarized in Table 1. For the wild type, the affinity for Ca^{2+} is between 0.4 and 1.0 ± 1.4 μM, which is slightly lower than previously reported ITC values of 0.8 ± 0.5 and 8.6 ± 1.1 μM.[8] The K_D values presented here are measured with twice as many data points and considered to be more accurate. However, the two-site independent binding model can give indistinguishable binding curves with completely different enthalpies and affinities.[28] The resulting affinities and enthalpies are therefore only approximate, as indicated by the large standard deviations. In the presence of 2 mM $MgCl_2$, the Ca^{2+} affinity of the remaining site is 3.4 ± 0.4 μM and the apparent affinity for Mg^{2+} in the presence of 90 μM $CaCl_2$ is 14.6 ± 3.4 μM. The Ca^{2+} binding affinity for the mutant is 16.1 ± 1.4 μM in the absence of $MgCl_2$ and 53.5 ± 9.70 μM in the presence of 2 mM $MgCl_2$. Unlike wt-CBD2, the D552V mutant does not display a Mg^{2+} binding isotherm in the presence of 90 μM $CaCl_2$.

Far-UV Circular Dichroism. In the absence of Ca^{2+}, Asp^{552} forms a salt bridge with Lys^{585}, and this interaction is deemed important for stabilizing CBD2.[8,15] To measure the stability of both wt- and D552V-CBD2, we followed the thermal unfolding using far-UV CD spectropolarimetry. We determined the melting temperatures (T_m) of both molecules in the presence of 1 mM EDTA, $CaCl_2$, or $MgCl_2$ (cf. Table 2 and Figure 3).

Table 2. Melting Temperatures (T_m) Determined by CD Spectropolarimetry at 1 mM $CaCl_2$, 1 mM $MgCl_2$, or 1 mM EDTA for wt-CBD2 and D552V-CBD2

condition	T_m for wt-CBD2 (°C)	T_m for D552V-CBD2 (°C)
1 mM EDTA	39.4 ± 1.1	30.9 ± 1.1
1 mM $MgCl_2$	55.8 ± 0.1	48.4 ± 0.1
1 mM $CaCl_2$	70.0 ± 0.1	57.1 ± 0.1

As expected, the T_m of the mutant in the apo form (30.9 ± 1.1 °C) is lower than that of the wild type (39.4 ± 1.1 °C), confirming the stabilizing function of Asp^{552}. Cation binding is also known to stabilize proteins,[29] and in accordance with that, we observe an increase in T_m from 39.4 ± 1.1 to 70.0 ± 0.1 °C when Ca^{2+} is bound to wt-CBD2. The T_m of Ca^{2+}-bound D5552V-CBD2 is 57.1 ± 0.1 °C, which is much lower than that of the Ca^{2+}-bound form of the wild type. In the presence of 1 mM $MgCl_2$, the T_m of wt-CBD2 is 55.8 ± 0.1 °C, an increase of 16.4 °C. Surprisingly, a similar increase in T_m of 17.5 °C is observed for D552V-CBD2 in the presence of 1 mM $MgCl_2$, as the mutant is not expected to bind Mg^{2+} in site II.

The increase in T_m at high Ca^{2+} and Mg^{2+} concentrations is due to binding of the ligand to the protein and therefore is expected to be dependent on ligand concentration. We followed the thermal unfolding using far-UV CD spectropolarimetry of both the wild type and mutant at eight different Mg^{2+} or Ca^{2+} concentrations at a constant total ionic strength and derived T_m, ΔH_m, and ΔC_p from the fits of the data (cf. Experimental Procedures). Figure 3C shows $1/T_m$ versus the common logarithm of the Ca^{2+} or Mg^{2+} concentration, whereas Figure S4 of the Supporting Information displays the values for ΔH_m and ΔC_p. As expected, we observe a strong ligand concentration dependence of the T_m. In addition, for both the wild type and the mutant, the first point that displays a significant decrease in $1/T_m$ is at 10 μM $CaCl_2$, whereas for $MgCl_2$, this point is at 100 μM. This indicates that the affinity for Mg^{2+} is much lower than that for Ca^{2+}.

NMR. To study the residue-specific effects of Mg^{2+} and Ca^{2+} binding, we measured the chemical shift perturbations (CSPs) on wt-CBD2 and D552V-CBD2, as induced by Mg^{2+} and Ca^{2+} using ^{15}N HSQC NMR spectroscopy. Spectra of both wt-CBD2 and D552V-CBD2 were measured at 10 different Mg^{2+}:protein ratios, from 0:1 to 26.4:1 (cf. Experimental Procedures). Subsequently, we performed a second titration using $CaCl_2$, in the presence of 10 mM $MgCl_2$, mimicking the

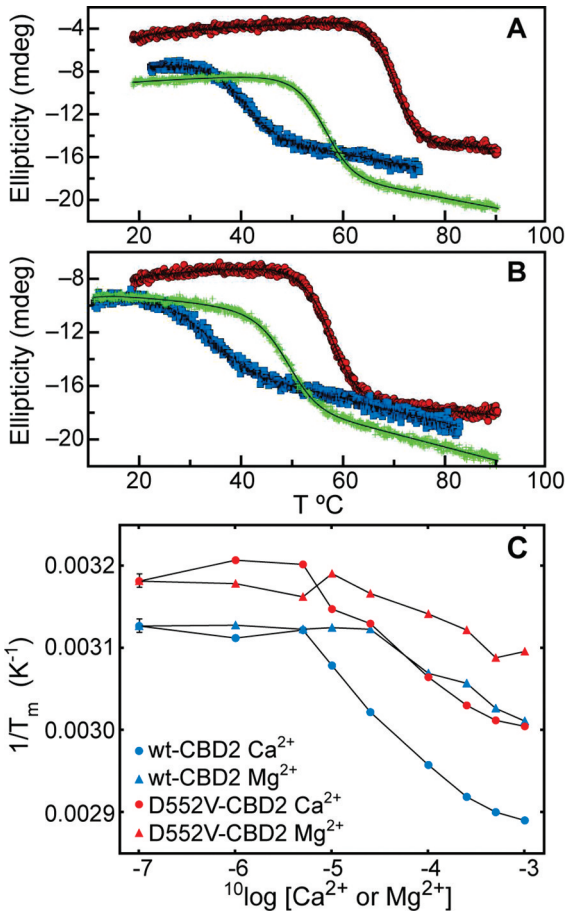

Figure 3. Thermal unfolding of wt-CBD2 (A) or D552V-CBD2 (B), examined by circular dichroism spectropolarimetry, in the presence of 1 mM $CaCl_2$ (red circles), 1 mM $MgCl_2$ (green crosses), or 1 mM EDTA (blue squares). (C) Ligand concentration dependence of T_m for Ca^{2+} (circles) and Mg^{2+} (triangles) for wt-CBD2 (blue) and D552V-CBD2 (red), where the 0 mM $CaCl_2$ or $MgCl_2$ data have been plotted at 10^{-7} M. The error estimates in T_m for all points are between 0.1 and 0.8 °C, which in most cases are smaller than the marker symbol. Hence, for the sake of clarity, only the largest error estimate is shown at the first data point.

ITC competition experiment described above (cf. Figure S3 of the Supporting Information).

To obtain residue ^{15}N HSQC assignments of D552V-CBD2 we conducted the standard triple-resonance experiments with D552V-CBD2 at 10 mM $CaCl_2$ (cf. Experimental Procedures) and assigned 113 of the 157 amides. Chemical shift information can be used to identify secondary structure elements, and we used the H^N, H^α, N, C^α, C^β, and CO assignments of D552V-CBD2 to perform a TALOS+[23] analysis. Even though the Asp^{552} to Val mutation destabilizes the domain, the TALOS +-derived φ and ψ backbone and S^2 order parameter predictions (cf. Figure S5 of the Supporting Information) show that the β-sandwich core remains intact.

Figure 4 displays the total CSP (cf. Experimental Procedures) upon addition of 10 mM $MgCl_2$ (panels A and C) and upon the subsequent addition of 10 mM $CaCl_2$ (panels B and D) as a function of residue number for wt-CBD2 and D552V-CBD2. The Mg^{2+}-induced CSPs observed in wt-CBD2 are not only around the CD binding loop (residues Glu^{543}–Thr^{556}) but also in the AB binding loop (residues Ser^{515}–Gly^{519}) located opposite of the CD loop (cf. Figure 1). Similarly, we find Mg^{2+} induced CSPs for D552V-CBD2 in the AB loop. Subsequent addition of $CaCl_2$ leads to chemical shift changes both in the wild type and in the mutant, indicating that Ca^{2+} binding still occurs even at high Mg^{2+} concentrations, a result that is in accordance with the ITC data. Furthermore, with the exception of those of Gly^{548} and Val^{575}, the largest CSPs during the Ca^{2+} titration are observed in the AB loop, located near Ca^{2+}-binding site I. Finally, when we derive the CSP as the difference between the apo and Ca^{2+}-bound forms at high Mg^{2+} concentrations, we observe values that are comparable with those reported previously[26] for the Ca^{2+}-bound form without Mg^{2+} (Figure 4C). This indicates that at 10 mM $MgCl_2$ and 10 mM $CaCl_2$, the binding sites are structurally similar as in the fully Ca^{2+}-bound form without Mg^{2+}.

Studying Mg^{2+} binding in more detail for wt-CBD2, we observe major differences between different residues. Six residues, Glu^{516}, Ser^{517}, Asp^{552}, Asp^{577}, Glu^{647}, and Glu^{648}, have large ^{15}N perturbations between the apo and fully ion-bound states and show significant exchange broadening during the Mg^{2+} titration. For these residues, the cross-peaks were broadened beyond detection at the third titration point (0.47:1 molar ratio) and reappear at the Ca^{2+}-bound position after titration of an excess of $CaCl_2$ (cf. Figure 5A,B). Three of these residues, Glu^{516}, Asp^{577}, and Glu^{648}, also exhibited exchange line broadening beyond detection in the regular Ca^{2+} titration, reported previously.[26] The cross-peaks of several other residues, for example, Ile^{518} and Gly^{548}, are clearly present at 10 mM Mg^{2+} and are approximately midway between the apo and Ca^{2+}-bound forms (cf. Figure 5C,D). Both types indicate that at high Mg^{2+} concentrations wt-CBD2 is in a state intermediate between an apo and fully ion-bound form. The most striking residues, however, show strongly curved trajectories during the Ca^{2+} titration. These residues, for example T556 and K653 (cf. Figure 5E,F), reveal that during the Ca^{2+} titration multiple processes occur, i.e., the binding of Ca^{2+} to site I and competition between Ca^{2+} and Mg^{2+} at site II and/or at site I at high Ca^{2+} concentrations.

To quantify the affinity of CBD2 for Mg^{2+}, we fitted a 1:1 binding model to the total CSPs of the selected individual residues (cf. Experimental Procedures). Some typical curves and the distribution of the resulting K_D values are shown in Figure S6 of the Supporting Information. The average K_D is 390 ± 260 μM. The large variation possibly originates from the fact that the chemical shift is sensitive to the structural, dynamic, and electronic environment of the nucleus, which do not affect all residues equally. The K_D of 390 ± 260 μM is not comparable to the K_D determined via ITC. However, in contrast to the ITC experiment, where Ca^{2+} is present in a 1:1 (Ca^{2+}:protein) ratio, the K_D values determined by NMR are derived under Ca^{2+}-free conditions. The strongly curved trajectories during the subsequent Ca^{2+} titration prohibited fitting of these curves in deriving a Ca^{2+} affinity in presence of 10 mM $MgCl_2$.

The apo and fully Ca^{2+}-bound forms of CBD2 are both structurally and dynamically different.[28] In the apo form, the binding loops of wt-CBD2 are more flexible and show decreased S^2 order parameters when compared to those of the Ca^{2+}-bound form. As a consequence, the overall tumbling is more anisotropic and the rotational correlation time is higher in the Ca^{2+}-bound form than in the apo form. We also tested the dynamic properties of the Mg^{2+}-bound form of wt-CBD2 and therefore measured the longitudinal (T_1) and transverse ($T_{1\rho}$)

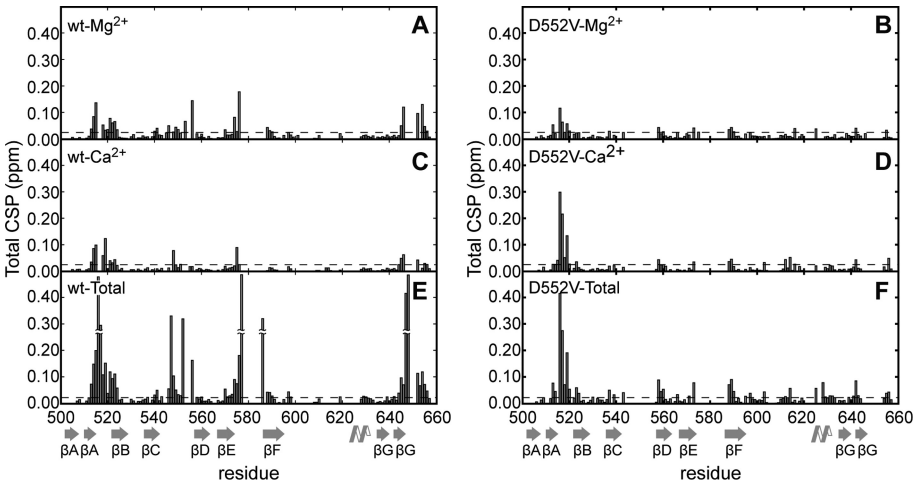

Figure 4. (A and B) CSP values as a function of residue number, resulting from 10 mM $MgCl_2$. (C and D) CSP values resulting from the difference between 10 mM $MgCl_2$ and 10 mM $CaCl_2$ in the presence of 10 mM $MgCl_2$. (E and F) Total CSP as the difference between 0 mM $MgCl_2$ and 10 mM $CaCl_2$ in the presence of 10 mM $MgCl_2$. For the sake of clarity, the sizes of the bars of Glu^{516}, Ser^{517}, Asp^{577}, Thr^{586}, Glu^{647}, and Glu^{648} have been reduced as indicated in the plot as these values exceed 0.5. These residues are not observed at 10 mM $MgCl_2$ in pane C (see also Results). Gray arrows denote β-strands, with the α-helix between β-strands F and G.

^{15}N relaxation times and the steady-state $^1H-^{15}N$ nuclear Overhauser effects of Mg^{2+}-bound wt-CBD2 (cf. Figure S7 of the Supporting Information). Analysis using Tensor2[27] (cf. Experimental Procedures) yielded values of $\tau_{av,aniso}$ and $D_{\parallel}/D_{\perp}$ (cf. Table 3) that show that the Mg^{2+}-bound form is dynamically intermediate between the apo and fully Ca^{2+}-bound forms (cf. Figure S8 of the Supporting Information). The mean S^2 value for the residues in the β-sandwich amounts to 0.95 ± 0.02, which is identical to the values of the other two forms. The mean S^2 value for the CD binding loop, however, is slightly increased compared to that of the apo form. The S^2 values for the other binding loops cannot be determined for the Mg^{2+}-bound form, as those peaks are missing due to exchange line broadening (vide supra).

DISCUSSION

Mg^{2+} is chemically very similar to Ca^{2+}, and many Ca^{2+}-binding proteins are known to bind Mg^{2+} to some extent. Thus far, most studies on ion specificity focused on EF-hand-containing proteins such as the calcium- and integrin-binding protein 1 parvalbumin (CIB1; see ref 30 for a review). CIB1, for example, binds Mg^{2+} at a position similar to that at which Ca^{2+} binds, and the Mg^{2+}−CIB1 complex is well-folded and structurally and dynamically very similar to the Ca^{2+}−CIB1 complex,[31] which raised the question of whether CIB can act as a Ca^{2+} sensor under physiological conditions.[32] In contrast, the Mg^{2+}-bound thymic avian hormone β-parvalbumin is structurally distinctly different from its Ca^{2+}-bound form,[33] and the two forms therefore have different binding partners.

How proteins are able to differentiate their affinities for different metal cations is still not fully understood, but on the basis of computational and experimental studies, some general trends have been identified. Both Mg^{2+} and Ca^{2+} are preferentially coordinated by carboxyl, carbonyl, and hydroxyl atoms.[34] However, Mg^{2+} strongly favors oxygen atoms in an octahedral fashion, whereas for Ca^{2+}, this can vary between six and eight. In addition, Mg^{2+} likes to retain several water molecules in its coordination sphere and prefers monodentate coordination of the side chain carboxylates. In contrast, Ca^{2+} has a lower affinity for water and has a tendency for coordination by bidentate carboxylates.[35] In accordance with this theory, it is to be expected that Mg^{2+} ions prefer site II over site I, as site II coordinates Ca^{2+} in a pentagonal bipyramidal fashion with five waters in the plane and the monodentate side chain oxygen atoms at almost perfect opposite positions (cf. Figure 1A).[15] It is reasonable to assume that Mg^{2+} at site II binds in a similar coordination, albeit with four instead of five waters, thereby maintaining its preferred octahedral coordination. Binding of Mg^{2+} at site I is much less optimal, as the coordination is far from octahedral and two bidentate coordination side chains are involved.

The ITC, CD, and NMR results of this study show that wt-CBD2 indeed binds Mg^{2+}, a finding in accordance with the results of Boyman et al.[14] To identify the binding site of Mg^{2+} and to obtain insight into the relative affinities of the two sites for the two ions, we constructed an Asp^{552} to Val mutant (D552V-CBD2), thereby removing one of the only two carboxylates coordinating the ion in site II. This mutation was previously shown to constitute a functional exchanger,[15] and the NMR data showed the overall fold of the D552V mutant to be similar to that of wt-CBD2, with only modest changes in the Ca^{2+} binding loops (cf. Figure S5 of the Supporting Information). Furthermore, the ITC results show that the D552V-CBD2 mutant binds only one Ca^{2+}, which demonstrates that site II has become nonfunctional and site I is still intact.

Direct titration of Mg^{2+} to wt-CBD2 gives only modest effects in the ITC (cf. Figure 2B), with a very low binding heat, possibly originating from energetically unfavorable breaking of the $Asp^{552}-Lys^{585}$ salt bridge. However, a high Mg^{2+} concentration reduces the Ca^{2+} binding stoichiometry of wt-CBD2 to 1:1, whereas the stoichiometry of D552V-CBD2 remains 1:1 under the same conditions. This effect can be reconciled by only a Ca^{2+} bound in site I and a Mg^{2+} ion in site II, which cannot be displaced by Ca^{2+}. The reverse experiment, titrating Mg^{2+} to a partially Ca^{2+}-loaded protein, resulted in a Mg^{2+} binding stoichiometry of 1:1 for wt-CBD2; no binding was observed for D552V-CBD2. Under these conditions, the ITC results show that Mg^{2+} binds at site II with a K_D of 14.6 ± 3.4 μM.

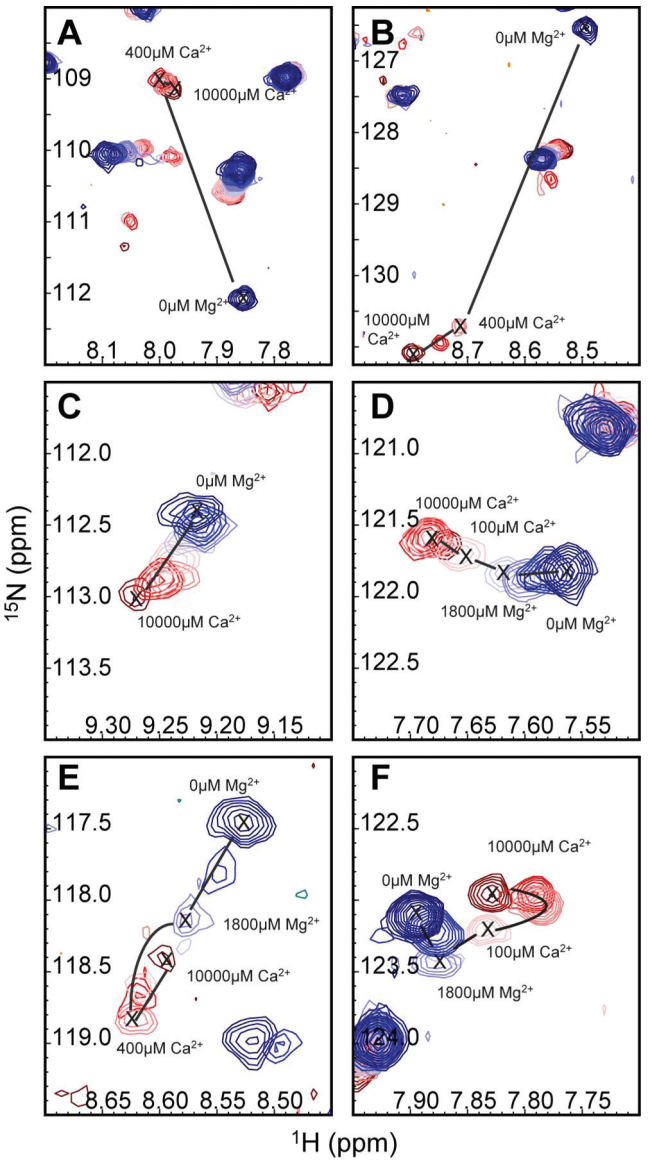

Figure 5. Mg^{2+} and Ca^{2+} titration of wt-CBD2 showing the overlays of eight ^{15}N HSQC spectra in the region of Ser^{517} (A), Asp^{577} (B), Ile^{518} (C), Gly^{548} (D), Thr^{556} (E), and Lys^{653} (F). In all panels, the concentrations are 0, 400, 1800, and 10000 μM $MgCl_2$ (dark blue to light blue) and 100, 400, 1800, and 10000 μM $CaCl_2$ (light pink to red).

Table 3. Overall Rotational Correlation Times and Anisotropies of Ca^{2+}-Bound, Mg^{2+}-Bound, and Apo wt-CBD2[a]

	Ca^{2+}-bound wt-CBD2	Mg^{2+}-bound wt-CBD2	apo wt-CBD2[a]
$\tau_{av,aniso}$ (ns)	13.1 ± 0.9	12.1 ± 0.91	11.4 ± 2.3
$D_{\parallel}/D_{\perp}$	2.08 ± 0.14	1.85 ± 0.33	1.4 ± 0.28

[a]Data from ref 26.

Using far-UV CD spectroscopy, we tested the thermal stability of the two domains in repsonse to varying concentrations of Ca^{2+} or Mg^{2+}. The CD results show that Mg^{2+} stabilizes wt-CBD2 compared to the apo form, with an increase in T_m of 16.4 °C, whereas for the fully Ca^{2+}-bound form, a 30.6 °C higher T_m is observed. Both Mg^{2+}- and Ca^{2+}-induced increases in T_m are strongly dependent on concentration. Even though an accurate determination of the binding affinities and stoichiometries from these data is not possible because of the large increase in ΔH_m (cf. Figure S4 of the Supporting Information),[36] Figure 3C clearly shows that for wt-CBD2 the affinity for Ca^{2+} is significantly higher than for Mg^{2+}. Surprisingly, a similar concentration-dependent increase in T_m at high $MgCl_2$ concentrations is found for D552V-CBD2 compared to that for wt-CBD2. This result also indicates that D552V-CBD2 is able to bind Mg^{2+}, resulting in increased stability of the domain. The exact location of this binding site is unclear; it could be at site I, at the defunct site II, or at the aspecific site also observed with the ITC at very high Ca^{2+} or Mg^{2+} concentrations (Figure S1 of the Supporting Information). However, the NMR chemical shift data of the mutant show a significant CSP between 0 and 10 mM $MgCl_2$ for the residues in the AB loop (Val^{514}–Ile^{518}), which suggests that in the mutant Mg^{2+} binds at site I, but with much lower affinity as Ca^{2+} can still replace the Mg^{2+}. This finding also explains the decrease in Ca^{2+} binding affinity and enthalpy for D552V-CBD2 at high $MgCl_2$ concentrations (cf. Table 1). The competition experiment allows for an estimate of the Mg^{2+} binding affinity for site I in D552V-CBD2 ($K_D \sim 860$ μM; cf. eq S8 of the Supporting Information[37]), which is in a range similar to that of the residue-specific K_D values derived via NMR.

Together, the ITC, NMR, and CD data show that Mg^{2+} binds to both sites I and II, albeit with significantly different affinities. Binding to site II is preferred by Mg^{2+} and displays the highest affinity ($K_D \sim 15$ μM), whereas site I has a much lower estimated Mg^{2+} binding affinity ($K_D \sim 300$–800 μM). Furthermore, in the Mg^{2+}-bound form of CBD2 (Mg^{2+}-CBD2), we observe many cross-peaks in the ^{15}N HSQC spectrum that are approximately midway between the apo and Ca^{2+}-bound forms. The results of the NMR relaxation studies show $\tau_{av,aniso}$ and $D_{\parallel}/D_{\perp}$ values that are exactly between those of the apo and fully Ca^{2+}-bound forms. This indicates that Mg^{2+}-CBD2 is in a state intermediate between the apo and fully Ca^{2+}-bound forms. Finally, the NMR results show that wt-CBD2 at high Ca^{2+} and Mg^{2+} concentrations, a condition in which wt-CBD2 is bound by one Mg^{2+} and one Ca^{2+}, is structurally very similar to the fully Ca^{2+}-bound form.

Previously, it was shown that the k_{on} rate for binding of Ca^{2+} to wt-CBD2 increases by a factor of more than 2 and the k_{off} rate decreases by almost 30% in the presence of Mg^{2+},[14] effectively increasing the affinity for Ca^{2+} by a factor of 2.5. Our results can explain these differences as binding of Mg^{2+} to site II also preforms site I. Both the NMR and X-ray structures of apo CBD2 (cf. Figure 1B,D) show that, in the absence of Ca^{2+}, the side chain of Lys^{585} is oriented toward to the now free site II, forming salt bridges with Asp^{552}. In addition, in the X-ray structure determined at pH 4.9, Lys^{585} forms another salt bridge with Glu^{648} and is hydrogen bonded to the carbonyl oxygen of Glu^{580}, displacing the EF loop toward the CD loop.[15] In spite of explicit examination of the relevant regions in the NOESY spectra of apo CBD2 recorded at pH 7.0, contacts from Lys^{585} to either Glu^{580} or Glu^{648} were not found.[16] Instead, NOEs to Glu^{582} were observed, and in the resulting NMR ensemble of apo CBD2, Lys^{585} is also engaged in a second salt bridge with Glu^{582}. This salt bridge occurs in only 8 of 20 structures of the ensemble as a result of a very flexible EF loop.[26] In either case, with Mg^{2+} bound at site II, the side chain of Lys^{585} will be displaced from the binding pocket, as a result of steric effects and repulsive interaction. Mg^{2+} binding at site II stabilizes the

dx.doi.org/10.1021/bi201134u | Biochemistry 2011, 50, 8804–8812

EF loop, and Asp[578] (coordinating Ca^{2+} in sites I and II in Ca^{2+}-CBD2) will be correctly oriented for coordination at site I. Therefore, Ca^{2+} can bind more easily at site I, explaining the higher k_{on} rate.

CBD2 plays an important role in the kinetic effects of NCX activation and displays a tight interplay with Na^+-dependent inactivation. Upon activation the exchanger, the current rapidly increases and then slowly decreases to a steady-state value as a result of Na^+-dependent inactivation. It has been postulated that at elevated Ca^{2+} concentrations, the level of Na^+-dependent inactivation is reduced through interactions with CBD2.[16] Assuming a cellular Mg^{2+} concentration of ~1.0 mM and Ca^{2+} concentrations between 100 nM at rest and 2.0 μM in the excited state, the apo form of CBD2 is hardly present under physiological conditions. Instead, the majority of the exchangers will have site II of CBD2 occupied with Mg^{2+}, which raises the question of whether this site is involved in the Ca^{2+} regulation of the intact NCX. More likely, site II bound by Mg^{2+} has a structuring role, increasing the Ca^{2+} binding rate of site I. In electrophysiological studies, Besserer et al. observed strongly altered Ca^{2+} regulation as a result of mutations affecting site I, whereas they did not observe significant effects for the D552V mutation.[15] Unfortunately, in that study as well as many others on the NCX, the concentrations of Mg^{2+} were not experimentally controlled. It would be interesting to know if and how these electrophysiological results would change in the presence of Mg^{2+}, especially with the respect to the rate of the regulatory response. The increase in affinity for Ca^{2+} at high Mg^{2+} concentrations[14] could also have an important effect in alleviating Na^+-dependent inactivation. We therefore hypothesize that at high Mg^{2+} concentrations the steady-state current of wt-CBD2 will be increased even at lower Ca^{2+} concentrations, whereas high Mg^{2+} concentrations will not exert any effect on the D552V mutant.

A constitutively bound Mg^{2+} at site II also affects the hypothesis of the electrostatic switch mechanism previously proposed, because apo CBD2 is not present under physiological conditions. If Ca^{2+} regulation occurs via electrostatic interactions, then differences in the electrostatic potential must be compared between one-ion Mg^{2+}-bound and fully Ca^{2+}-bound CBD2. Calculating the electrostatic potential by ABPS[38] using one ion present at site II shows that differences still exist between Mg^{2+}-bound CBD2 and Ca^{2+}-bound CBD2; however, the differences are much smaller compared to apo CBD2 (Figure S9 of the Supporting Information). Another complicating factor is the protonation state of the charged residues. In the electrostatic calculations, all Asp and Glu side chains are fully deprotonated, as the predicted pK_a of all Asp and Glu side chains is smaller than 4.8 (calculated using PROPKA,[39,40] data not shown). However, a recent study shows that the Ca^{2+} affinity of CBD2 decreases 24% when the pH is lowered from 7.2 to 6.9.[41] Possibly not all side chains are actually fully deprotonated at decreased pH, and the authors further suggest that the protonation state changes upon Ca^{2+} binding. Unfortunately, no data about interactions between H^+ and Mg^{2+} are available, but we speculate that proton sensitivity decreases with Mg^{2+} bound at site II, as binding of the first ion may deprotonate (or keep deprotonated) the coordinating residues of the other site.

Our study unequivocally shows that CBD2-AD of NCX1 binds Mg^{2+} at a concentration far below the physiological $MgCl_2$ concentration of ~1 mM. Both site I and site II bind Mg^{2+}, although with significantly different affinities. The different isoforms and splice variants of the NCX change the number of Ca^{2+} ions bound by CBD2, likely altering the regulation to tissue-specific needs. Whether Mg^{2+} will bind to CBD2 of other NCX isoforms as well as to CBD1 and tranport sites remains to be established. Finally, our study shows that Mg^{2+} has a stabilizing and structural effect on CBD2 of NCX1, and we suggest that physiological experiments hould be performed at controlled Mg^{2+} concentrations for obtaining relevant results regarding regulation of the exchanger.

■ ASSOCIATED CONTENT

Ⓢ Supporting Information

Detailed procedure for the fitting of the NMR titration and far-UV CD data, ITC data for wt- and D552V-CBD2D at high $CaCl_2$ or $MgCl_2$ concentrations and at 2 mM choline chloride, ^{15}N HSQC overlays of wt- and D552V-CBD2 without Mg^{2+} or Ca^{2+} or with 10 mM $MgCl_2$ and 10 mM $CaCl_2$, ^{15}N backbone relaxation rates of R_1, $R_{1\rho}$, and NOE per residue of wt-CBD2 at 10 mM $MgCl_2$, Tensor2-derived model-free parameters of these relaxation rates, and electrostatic potentials of apo, Mg^{2+}-bound, and Ca^{2+}-saturated CBD2-AD. This material is available free of charge via the Internet at http://pubs.acs.org.

■ AUTHOR INFORMATION

Corresponding Author

*Department of Biochemistry, University of Leicester, Lancaster Road, Leicester LE1 9HN, U.K. Telephone: +44 116 229 7076. Fax: +44 116 229 7018. E-mail: gv29@le.ac.uk.

Funding

This research was supported by The Netherlands Organization for Scientific Research (NWO) Grants 700.55.443 and 700.57.101.

■ ACKNOWLEDGMENTS

We thank Ing. Nathalie Schilderink for expert assistance with the CBD2 production and purification and Marco Felici for help with the backbone assignment of D552V-CBD2.

■ ABBREVIATIONS

CBD1, Ca^{2+}-binding domain 1; CBD2, Ca^{2+}-binding domain 2; CD, circular dichroism; CLD, α-catenin-like domain; CSP, chemical shift perturbation; ITC, isothermal titration calorimetry; HSQC, heteronuclear single-quantum correlation; NCX, Na^+-Ca^{2+} exchanger; NOE, nuclear Overhauser effect; NOESY, nuclear Overhauser effect spectroscopy; NMR, nuclear magnetic resonance; PDB, Protein Data Bank.

■ REFERENCES

(1) Quednau, B. D., Nicoll, D. A., and Philipson, K. D. (1996) Tissue-specific expression of the Na/Ca exchanger isoforms NCX1, NCX2, and NCX3. *Biophys. J.*, MP282.

(2) Egger, M., and Niggli, E. (1999) Regulatory function of Na-Ca exchange in the heart: Milestones and outlook. *J. Membr. Biol. 168*, 107−130.

(3) Lytton, J. (2007) Na^+/Ca^{2+} exchangers: Three mammalian gene families control Ca^{2+} transport. *Biochem. J. 406*, 365−382.

(4) Kang, T. M., and Hilgemann, D. W. (2004) Multiple transport modes of the cardiac Na^+/Ca^{2+} exchanger. *Nature 427*, 544−548.

(5) Hilgemann, D. W., Matsuoka, S., Nagel, G. A., and Collins, A. (1992) Steady-state and dynamic properties of cardiac sodium-calcium exchange. Sodium-dependent inactivation. *J. Gen. Physiol. 100*, 905−932.

(6) Iwamoto, T., Nakamura, T. Y., Pan, Y., Uehara, A., Imanaga, I., and Shigekawa, M. (1999) Unique topology of the internal repeats in the cardiac Na^+/Ca^{2+} exchanger. *FEBS Lett. 446*, 264−268.
(7) Nicoll, D. A., Ottolia, M., Lu, L. Y., Lu, Y. J., and Philipson, K. D. (1999) A new topological model of the cardiac sarcolemmal Na^+-Ca^{2+} exchanger. *J. Biol. Chem. 274*, 910−917.
(8) Hilge, M., Aelen, J., and Vuister, G. W. (2006) Ca^{2+} regulation in the Na^+/Ca^{2+} exchanger involves two markedly different Ca^{2+} sensors. *Mol. Cell 22*, 15−25.
(9) Saris, N. E. L., Mervaala, E., Karppanen, H., Khawaja, J. A., and Lewenstam, A. (2000) Magnesium: An update on physiological, clinical and analytical aspects. *Clin. Chim. Acta 294*, 1−26.
(10) Laude, A. J., and Simpson, A. W. M. (2009) Compartmentalized signalling: Ca^{2+} compartments, microdomains and the many facets of Ca^{2+} signalling. *FEBS J. 276*, 1800−1816.
(11) DiPolo, R., and Beauge, L. (2008) In the squid axon Na^+/Ca^{2+} exchanger the state of the Ca-i-regulatory site influences the affinities of the intra- and extracellular transport sites for Na^+ and Ca^{2+}. *Pfluegers Arch. 456*, 623−633.
(12) Levitsky, D. O., Nicoll, D. A., and Philipson, K. D. (1994) Identification of the high-affinity Ca^{2+}-binding domain of the cardiac Na^+-Ca^{2+} exchanger. *J. Biol. Chem. 269*, 22847−22852.
(13) Wei, S. K., Quigley, J. F., Hanlon, S. U., O'Rourke, B., and Haigney, M. C. P. (2002) Cytosolic free magnesium modulates Na/Ca exchange currents in pig myocytes. *Cardiovasc. Res. 53*, 334−340.
(14) Boyman, L., Mikhasenko, H., Hiller, R., and Khananshvili, D. (2009) Kinetic and equilibrium properties of regulatory calcium sensors of NCX1 protein. *J. Biol. Chem. 284*, 6185−6193.
(15) Besserer, G. M., Ottolia, M., Nicoll, D. A., Chaptal, V., Cascio, D., Philipson, K. D., and Abramson, J. (2007) The second Ca^{2+}-binding domain of the Na^+-Ca^{2+} exchanger is essential for regulation: Crystal structures and mutational analysis. *Proc. Natl. Acad. Sci. U.S.A. 104*, 18467−18472.
(16) Hilge, M., Aelen, J., Foarce, A., Perrakis, A., and Vuister, G. W. (2009) Ca^{2+} regulation in the Na^+/Ca^{2+} exchanger features a dual electrostatic switch mechanism. *Proc. Natl. Acad. Sci. U.S.A. 106*, 14333−14338.
(17) Nicoll, D. A., Sawaya, M. R., Kwon, S., Cascio, D., Philipson, K. D., and Abramson, J. (2006) The crystal structure of the primary Ca^{2+} sensor of the Na^+/Ca^{2+} exchanger reveals a novel Ca^{2+} binding motif. *J. Biol. Chem. 281*, 21577−21581.
(18) Wu, M., Le, H. D., Wang, M., Yurkov, V., Omelchenko, A., Hnatowich, M., Nix, J., Hryshko, L. V., and Zheng, L. (2010) Crystal Structures of Progressive Ca^{2+} Binding States of the Ca^{2+} Sensor Ca^{2+} Binding Domain 1 (CBD1) from the CALX Na^+/Ca^{2+} Exchanger Reveal Incremental Conformational Transitions. *J. Biol. Chem. 285*, 2554−2561.
(19) Wu, M., Wang, M., Nix, J., Hryshko, L. V., and Zheng, L. (2009) Crystal Structure of CBD2 from the *Drosophila* Na^+/Ca^{2+} Exchanger: Diversity of Ca^{2+} Regulation and Its Alternative Splicing Modification. *J. Mol. Biol. 387*, 104−112.
(20) Delaglio, F., Grzesiek, S., Vuister, G. W., Zhu, G., Pfeifer, J., and Bax, A. (1995) NMRPipe: A multidimensional spectral processing system based on UNIX pipes. *J. Biomol. NMR 6*, 277−293.
(21) Vranken, W. F., Boucher, W., Stevens, T. J., Fogh, R. H., Pajon, A., Llinas, P., Ulrich, E. L., Markley, J. L., Ionides, J., and Laue, E. D. (2005) The CCPN data model for NMR spectroscopy: Development of a software pipeline. *Proteins 59*, 687−696.
(22) *The PyMOL Molecular Graphics System*, version 1.3r1 (2010) Schrödinger, LLC, New York.
(23) Shen, Y., Delaglio, F., Cornilescu, G., and Bax, A. (2009) TALOS+: A hybrid method for predicting protein backbone torsion angles from NMR chemical shifts. *J. Biomol. NMR 44*, 213−223.
(24) Ayed, A., Mulder, F. A. A., Yi, G. S., Lu, Y., Kay, L. E., and Arrowsmith, C. H. (2001) Latent and active p53 are identical in conformation. *Nat. Struct. Biol. 8*, 756−760.
(25) André, I., and Linse, S. (2002) Measurement of Ca^{2+}-binding constants of proteins and presentation of the CaLigator software. *Anal. Biochem. 305*, 195−205.
(26) Breukels, V., and Vuister, G. W. (2010) Binding of calcium is sensed structurally and dynamically throughout the second calcium-binding domain of the sodium/calcium exchanger. *Proteins 78*, 1813−1824.
(27) Dosset, P., Hus, J. C., Blackledge, M., and Marion, D. (2000) Efficient analysis of macromolecular rotational diffusion from heteronuclear relaxation data. *J. Biomol. NMR 16*, 23−28.
(28) Freire, E., Schön, A., and Velazquez-Campoy, A. (2009) Isothermal titration calorimetry: General formalism using binding polynomials. *Methods Enzymol. 455*, 127−155.
(29) Pace, C. N. (1990) Measuring and increasing protein stability. *Trends Biotechnol. 8*, 93−98.
(30) Gifford, J. L., Walsh, M. P., and Vogel, H. J. (2007) Structures and metal-ion-binding properties of the Ca^{2+}-binding helix-loop-helix EF-hand motifs. *Biochem. J. 405*, 199−221.
(31) Yamniuk, A. P., Gifford, J. L., Linse, S., and Vogel, H. J. (2008) Effects of metal-binding loop mutations on ligand binding to calcium- and integrin-binding protein 1. Evolution of the EF-hand. *Biochemistry 47*, 1696−1707.
(32) Yamniuk, A. P., and Vogel, H. J. (2005) Calcium- and magnesium-dependent interactions between calcium- and integrin-binding protein and the integrin α IIb cytoplasmic domain. *Protein Sci. 14*, 1429−1437.
(33) Tan, A., and Henzl, M. T. (2009) Evidence for a Ca^{2+}-Specific Conformational Change in Avian Thymic Hormone, a High-Affinity β-Parvalbumin. *Biochemistry 48*, 3936−3945.
(34) Dokmanic, I., Sikic, M., and Tomic, S. (2008) Metals in proteins: Correlation between the metal-ion type, coordination number and the amino-acid residues involved in the coordination. *Acta Crystallogr. D64*, 257−263.
(35) Dudev, T., and Lim, C. (2003) Principles governing Mg, Ca, and Zn binding and selectivity in proteins. *Chem. Rev. 103*, 773−787.
(36) Greenfield, N. J. (2006) Using circular dichroism collected as a function of temperature to determine the thermodynamics of protein unfolding and binding interactions. *Nat. Protoc. 1*, 2527−2535.
(37) Malmendal, A., Linse, S., Evenäs, J., Forsén, S., and Drakenberg, T. (1999) Battle for the EF-hands: Magnesium-calcium interference in calmodulin. *Biochemistry 38*, 11844−11850.
(38) Baker, N. A., Sept, D., Joseph, S., Holst, M. J., and McCammon, J. A. (2001) Electrostatics of nanosystems: Application to microtubules and the ribosome. *Proc. Natl. Acad. Sci. U.S.A. 98*, 10037−10041.
(39) Bas, D. C., Rogers, D. M., and Jensen, J. H. (2008) Very fast prediction and rationalization of pKa values for protein-ligand complexes. *Proteins 73*, 765−783.
(40) Li, H., Robertson, A. D., and Jensen, J. H. (2005) Very fast empirical prediction and rationalization of protein pKa values. *Proteins 61*, 704−721.
(41) Boyman, L., Hagen, B. M., Giladi, M., Hiller, R., Lederer, W. J., and Khananshvili, D. (2011) Proton-sensing Ca^{2+} Binding Domains Regulate the Cardiac Na^+/Ca^{2+} Exchanger. *J. Biol. Chem. 286*, 28811−28820.
(42) Spronk, C. A. E. M., Linge, J. P., Hilbers, C. W., and Vuister, G. W. (2002) Improving the quality of protein structures derived by NMR spectroscopy. *J. Biomol. NMR 22*, 281−289.